ELSEVIER

Physics Letters B 537 (2002) 5–20

PHYSICS LETTERS B

www.elsevier.com/locate/npe

Search for scalar quarks in e^+e^- collisions at $\sqrt{s}$ up to 209 GeV

ALEPH Collaboration

A. Heister, S. Schael

Physikalisches Institut das RWTH-Aachen, D-52056 Aachen, Germany

R. Barate, R. Brunelière, I. De Bonis, D. Decamp, C. Goy, S. Jezequel, J.-P. Lees, F. Martin, E. Merle, M.-N. Minard, B. Pietrzyk, B. Trocmé

Laboratoire de Physique des Particules (LAPP), IN^2P^3-CNRS, F-74019 Annecy-le-Vieux Cedex, France

G. Boix [25], S. Bravo, M.P. Casado, M. Chmeissani, J.M. Crespo, E. Fernandez, M. Fernandez-Bosman, Ll. Garrido [15], E. Graugés, J. Lopez, M. Martinez, G. Merino, R. Miquel [4], Ll.M. Mir [4], A. Pacheco, D. Paneque, H. Ruiz

Institut de Física d'Altes Energies, Universitat Autònoma de Barcelona, E-08193 Bellaterra (Barcelona), Spain [7]

A. Colaleo, D. Creanza, N. De Filippis, M. de Palma, G. Iaselli, G. Maggi, M. Maggi, S. Nuzzo, A. Ranieri, G. Raso [24], F. Ruggieri, G. Selvaggi, L. Silvestris, P. Tempesta, A. Tricomi [3], G. Zito

Dipartimento di Fisica, INFN Sezione di Bari, I-70126 Bari, Italy

X. Huang, J. Lin, Q. Ouyang, T. Wang, Y. Xie, R. Xu, S. Xue, J. Zhang, L. Zhang, W. Zhao

Institute of High Energy Physics, Academia Sinica, Beijing, People's Republic of China [8]

D. Abbaneo, P. Azzurri, T. Barklow [30], O. Buchmüller [30], M. Cattaneo, F. Cerutti, B. Clerbaux [34], H. Drevermann, R.W. Forty, M. Frank, F. Gianotti, T.C. Greening [26], J.B. Hansen, J. Harvey, D.E. Hutchcroft, P. Janot, B. Jost, M. Kado [2], P. Mato, A. Moutoussi, F. Ranjard, L. Rolandi, D. Schlatter, G. Sguazzoni, W. Tejessy, F. Teubert, A. Valassi, I. Videau, J.J. Ward

European Laboratory for Particle Physics (CERN), CH-1211 Geneva 23, Switzerland

0370-2693/02/$ – see front matter
PII: S0370-2693(02)01827-0

F. Badaud, S. Dessagne, A. Falvard [20], D. Fayolle, P. Gay, J. Jousset, B. Michel, S. Monteil, D. Pallin, J.M. Pascolo, P. Perret

Laboratoire de Physique Corpusculaire, Université Blaise Pascal, IN^2P^3-CNRS, Clermont-Ferrand, F-63177 Aubière, France

J.D. Hansen, J.R. Hansen, P.H. Hansen, B.S. Nilsson

Niels Bohr Institute, 2100 Copenhagen, DK-Denmark [9]

A. Kyriakis, C. Markou, E. Simopoulou, A. Vayaki, K. Zachariadou

Nuclear Research Center Demokritos (NRCD), GR-15310 Attiki, Greece

A. Blondel [12], J.-C. Brient, F. Machefert, A. Rougé, M. Swynghedauw, R. Tanaka, H. Videau

Laboratoire de Physique Nucléaire et des Hautes Energies, Ecole Polytechnique, IN^2P^3-CNRS, F-91128 Palaiseau Cedex, France

V. Ciulli, E. Focardi, G. Parrini

Dipartimento di Fisica, Università di Firenze, INFN Sezione di Firenze, I-50125 Firenze, Italy

A. Antonelli, M. Antonelli, G. Bencivenni, F. Bossi, G. Capon, V. Chiarella, P. Laurelli, G. Mannocchi [5], G.P. Murtas, L. Passalacqua

Laboratori Nazionali dell'INFN (LNF-INFN), I-00044 Frascati, Italy

J. Kennedy, J.G. Lynch, P. Negus, V. O'Shea, A.S. Thompson

Department of Physics and Astronomy, University of Glasgow, Glasgow G12 8QQ, United Kingdom [10]

S. Wasserbaech

Department of Physics, Haverford College, Haverford, PA 19041-1392, USA

R. Cavanaugh [33], S. Dhamotharan [21], C. Geweniger, P. Hanke, V. Hepp, E.E. Kluge, G. Leibenguth, A. Putzer, H. Stenzel, K. Tittel, M. Wunsch [19]

Kirchhoff-Institut für Physik, Universität Heidelberg, D-69120 Heidelberg, Germany [16]

R. Beuselinck, W. Cameron, G. Davies, P.J. Dornan, M. Girone [1], R.D. Hill, N. Marinelli, J. Nowell, S.A. Rutherford, J.K. Sedgbeer, J.C. Thompson [14], R. White

Department of Physics, Imperial College, London SW7 2BZ, United Kingdom [10]

V.M. Ghete, P. Girtler, E. Kneringer, D. Kuhn, G. Rudolph

Institut für Experimentalphysik, Universität Innsbruck, A-6020 Innsbruck, Austria [18]

E. Bouhova-Thacker, C.K. Bowdery, D.P. Clarke, G. Ellis, A.J. Finch, F. Foster, G. Hughes, R.W.L. Jones, M.R. Pearson, N.A. Robertson, M. Smizanska

Department of Physics, University of Lancaster, Lancaster LA1 4YB, United Kingdom [10]

O. van der Aa, C. Delaere, V. Lemaitre

Institut de Physique Nucléaire, Département de Physique, Université Catholique de Louvain, 1348 Louvain-la-Neuve, Belgium

U. Blumenschein, F. Hölldorfer, K. Jakobs, F. Kayser, K. Kleinknecht, A.-S. Müller, G. Quast [6], B. Renk, H.-G. Sander, S. Schmeling, H. Wachsmuth, C. Zeitnitz, T. Ziegler

Institut für Physik, Universität Mainz, D-55099 Mainz, Germany [16]

A. Bonissent, P. Coyle, C. Curtil, A. Ealet, D. Fouchez, P. Payre, A. Tilquin

Centre de Physique des Particules de Marseille, Univ. Méditerranée, IN^{2}P^3-CNRS, F-13288 Marseille, France

F. Ragusa

Dipartimento di Fisica, Università di Milano e INFN Sezione di Milano, I-20133 Milano, Italy

A. David, H. Dietl, G. Ganis [27], K. Hüttmann, G. Lütjens, W. Männer, H.-G. Moser, R. Settles, G. Wolf

Max-Planck-Institut für Physik, Werner-Heisenberg-Institut, D-80805 München, Germany [16]

J. Boucrot, O. Callot, M. Davier, L. Duflot, J.-F. Grivaz, Ph. Heusse, A. Jacholkowska [32], C. Loomis, L. Serin, J.-J. Veillet, J.-B. de Vivie de Régie [28], C. Yuan

Laboratoire de l'Accélérateur Linéaire, Université de Paris-Sud, IN^{2}P^3-CNRS, F-91898 Orsay Cedex, France

G. Bagliesi, T. Boccali, L. Foà, A. Giammanco, A. Giassi, F. Ligabue, A. Messineo, F. Palla, G. Sanguinetti, A. Sciabà, R. Tenchini [1], A. Venturi [1], P.G. Verdini

Dipartimento di Fisica dell'Università, INFN Sezione di Pisa, e Scuola Normale Superiore, I-56010 Pisa, Italy

O. Awunor, G.A. Blair, G. Cowan, A. Garcia-Bellido, M.G. Green, L.T. Jones, T. Medcalf, A. Misiejuk, J.A. Strong, P. Teixeira-Dias

Department of Physics, Royal Holloway & Bedford New College, University of London, Egham, Surrey TW20 OEX, United Kingdom [10]

R.W. Clifft, T.R. Edgecock, P.R. Norton, I.R. Tomalin

Particle Physics Dept., Rutherford Appleton Laboratory, Chilton, Didcot, Oxon OX11 OQX, United Kingdom [10]

B. Bloch-Devaux, D. Boumediene, P. Colas, B. Fabbro, E. Lançon, M.-C. Lemaire, E. Locci, P. Perez, J. Rander, B. Tuchming, B. Vallage

CEA, DAPNIA/Service de Physique des Particules, CE-Saclay, F-91191 Gif-sur-Yvette Cedex, France [17]

N. Konstantinidis, A.M. Litke, G. Taylor

Institute for Particle Physics, University of California at Santa Cruz, Santa Cruz, CA 95064, USA [22]

C.N. Booth, S. Cartwright, F. Combley [31], P.N. Hodgson, M. Lehto, L.F. Thompson

Department of Physics, University of Sheffield, Sheffield S3 7RH, United Kingdom [10]

K. Affholderbach [23], A. Böhrer, S. Brandt, C. Grupen, J. Hess, A. Ngac, G. Prange, U. Sieler

Fachbereich Physik, Universität Siegen, D-57068 Siegen, Germany [16]

C. Borean, G. Giannini

Dipartimento di Fisica, Università di Trieste e INFN Sezione di Trieste, I-34127 Trieste, Italy

H. He, J. Putz, J. Rothberg

Experimental Elementary Particle Physics, University of Washington, Seattle, WA 98195, USA

S.R. Armstrong, K. Berkelman, K. Cranmer, D.P.S. Ferguson, Y. Gao [29], S. González, O.J. Hayes, H. Hu, S. Jin, J. Kile, P.A. McNamara III, J. Nielsen, Y.B. Pan, J.H. von Wimmersperg-Toeller, W. Wiedenmann, J. Wu, Sau Lan Wu, X. Wu, G. Zobernig

Department of Physics, University of Wisconsin, Madison, WI 53706, USA [11]

G. Dissertori

Institute for Particle Physics, ETH Hönggerberg, 8093 Zürich, Switzerland

Received 23 January 2002; accepted 18 April 2002

Editor: L. Montanet

Abstract

Searches for scalar top, scalar bottom and mass-degenerate scalar quarks are performed in the data collected by the ALEPH detector at LEP, at centre-of-mass energies up to 209 GeV, corresponding to an integrated luminosity of 675 pb^{-1}. No evidence for the production of such particles is found in the decay channels $\tilde{\mathrm{t}} \to \mathrm{c}/\mathrm{u}\chi$, $\tilde{\mathrm{t}} \to \mathrm{b}\ell\tilde{\nu}$, $\tilde{\mathrm{b}} \to \mathrm{b}\chi$, $\tilde{\mathrm{q}} \to \mathrm{q}\chi$ or in the stop four-body decay channel $\tilde{\mathrm{t}} \to \mathrm{b}\chi\mathrm{f}\bar{\mathrm{f}}'$ studied for the first time at LEP. The results of these searches yield improved mass lower limits. In particular, an absolute lower limit of 63 GeV/c^2 is obtained for the stop mass, at 95% confidence level, irrespective of the stop lifetime and decay branching ratios.

[1] Also at CERN, 1211 Geneva 23, Switzerland.
[2] Now at Fermilab, PO Box 500, MS 352, Batavia, IL 60510, USA.
[3] Also at Dipartimento di Fisica di Catania and INFN Sezione di Catania, 95129 Catania, Italy.
[4] Now at LBNL, Berkeley, CA 94720, USA.
[5] Also Istituto di Cosmo-Geofisica del CNR, Torino, Italy.
[6] Now at Institut für Experimentelle Kernphysik, Universität Karlsruhe, 76128 Karlsruhe, Germany.
[7] Supported by CICYT, Spain.
[8] Supported by the National Science Foundation of China.
[9] Supported by the Danish Natural Science Research Council.
[10] Supported by the UK Particle Physics and Astronomy Research Council.
[11] Supported by the US Department of Energy, grant DE-FG0295-ER40896.
[12] Now at Departement de Physique Corpusculaire, Université de Genève, 1211 Genève 4, Switzerland.
[13] Supported by the Commission of the European Communities, contract ERBFMBICT982874.
[14] Supported by the Leverhulme Trust.
[15] Permanent address: Universitat de Barcelona, 08208 Barcelona, Spain.
[16] Supported by Bundesministerium für Bildung und Forschung, Germany.
[17] Supported by the Direction des Sciences de la Matière, CEA.
[18] Supported by the Austrian Ministry for Science and Transport.
[19] Now at SAP AG, 69185 Walldorf, Germany.
[20] Now at Groupe d'Astroparticules de Montpellier, Université de Montpellier II, 34095 Montpellier, France.
[21] Now at BNP Paribas, 60325 Frankfurt am Mainz, Germany.
[22] Supported by the US Department of Energy, grant DE-FG03-92ER40689.
[23] Now at Skyguide, Swissair Navigation Services, Geneva, Switzerland.
[24] Also at Dipartimento di Fisica e Tecnologie Relative, Università di Palermo, Palermo, Italy.
[25] Now at McKinsey and Compagny, Avenue Louis Casal 18, 1203 Geneva, Switzerland.
[26] Now at Honeywell, Phoenix AZ, USA.
[27] Now at INFN Sezione di Roma II, Dipartimento di Fisica, Università di Roma Tor Vergata, 00133 Roma, Italy.
[28] Now at Centre de Physique des Particules de Marseille, Univ. Méditerranée, F-13288 Marseille, France.
[29] Also at Department of Physics, Tsinghua University, Beijing, People's Republic of China.
[30] Now at SLAC, Stanford, CA 94309, USA.
[31] Deceased.
[32] Also at Groupe d'Astroparticules de Montpellier, Université de Montpellier II, 34095 Montpellier, France.
[33] Now at University of Florida, Department of Physics, Gainesville, Florida 32611-8440, USA.
[34] Now at Institut Inter-universitaire des hautes Energies (IIHE), CP 230, Université Libre de Bruxelles, 1050 Bruxelles, Belgique.

1. Introduction

The results of searches for scalar quarks with the data collected in the year 2000 by the ALEPH detector at LEP are presented in this Letter. The energies and integrated luminosities of the analysed data samples are given in Table 1. Previous results obtained with lower energy data have been reported by ALEPH in Refs. [1–5] and by the other LEP Collaborations in Refs. [6–8].

The theoretical framework for these studies is the supersymmetric extension of the Standard Model [9], with R-parity conservation. The lightest supersymmetric particle (LSP) is assumed to be the lightest neutralino χ or the sneutrino $\tilde{\nu}$. Such an LSP is stable and weakly interacting. Each chirality state of the Standard Model fermions has a scalar supersymmetric partner. The scalar quarks (squarks) $\tilde{q}_L$ and $\tilde{q}_R$ are the supersymmetric partners of the left-handed and right-handed quarks, respectively. The mass eigenstates are orthogonal combinations of the weak interaction eigenstates $\tilde{q}_L$ and $\tilde{q}_R$. The mixing angle $\theta_{\tilde{q}}$ is defined in such a way that $\tilde{q} = \tilde{q}_L \cos\theta_{\tilde{q}} + \tilde{q}_R \sin\theta_{\tilde{q}}$ is the lighter squark. The off-diagonal terms of the mass matrix, responsible for mixing, read, with standard notation: $m_q(A_q - \mu\kappa)$, with $\kappa = \tan\beta$ for down-type and $\kappa = 1/\tan\beta$ for up-type quarks. Since the size of this mixing term is proportional to the mass of the Standard Model partner, it could well be that the lightest supersymmetric charged particle is the lighter scalar top (stop, $\tilde{t}$) or, in particular for large $\tan\beta$ values, the lighter scalar bottom (sbottom, $\tilde{b}$). Squarks could be produced at LEP in pairs, $e^+e^- \to \tilde{q}\bar{\tilde{q}}$, via s-channel exchange of a virtual photon or Z. The production cross section [10] depends on $\theta_{\tilde{q}}$ when mixing is relevant, i.e., for stops and sbottoms.

Table 1
Integrated luminosities, centre-of-mass energy ranges and mean centre-of-mass energy values for the data collected by the ALEPH detector in the year 2000

Luminosity (pb^{-1})	Energy range (GeV)	$\langle\sqrt{s}\rangle$ (GeV)
9.4	207–209	208.0
122.6	206–207	206.6
75.3	204–206	205.2

The searches for stops described here assume that all supersymmetric particles except the lightest neutralino χ and possibly the sneutrino $\tilde{\nu}$ are heavier than the stop. Under these assumptions, the allowed decay channels are $\tilde{t} \to c/u\chi$, $\tilde{t} \to b\chi f\bar{f}'$ and $\tilde{t} \to b\ell\tilde{\nu}$ [10,11]. The corresponding diagrams are shown in Fig. 1. The decay $\tilde{t} \to c\chi$ (Fig. 1(a)) proceeds only via loops and has a very small width, of the order of 0.01–1 eV [10], depending on the mass difference ΔM between the stop and the neutralino, and on the masses and field content of the particles involved in the loops. For low enough ΔM values ($\Delta M \lesssim 6$ GeV/c^2), the stop lifetime becomes sizeable, and must be taken into account in the searches for stop production. If ΔM is so small that the $\tilde{t} \to c\chi$ channel is kinematically closed, the dominant decay mode becomes $\tilde{t} \to u\chi$, and the stop can then be considered as stable for practical purposes.

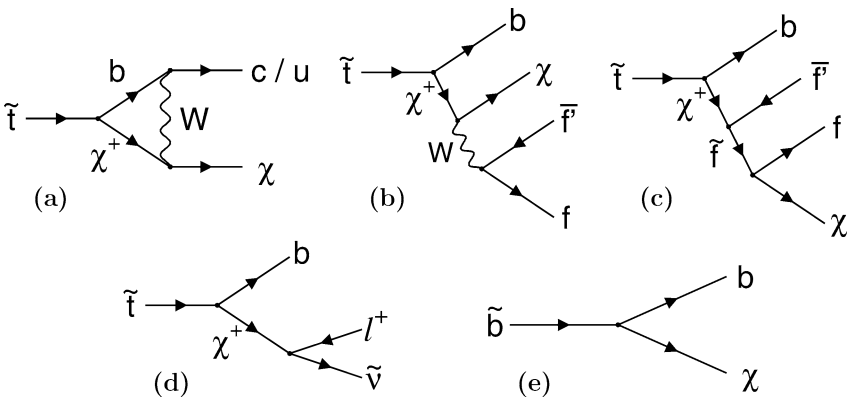

Fig. 1. Squark decay diagrams considered in this Letter: (a) $\tilde{t} \to c/u\chi$; (b) $\tilde{t} \to b\chi f\bar{f}'$ via W exchange and (c) $\tilde{t} \to b\chi f\bar{f}'$ via sfermion exchange; (d) $\tilde{t} \to b\ell\tilde{\nu}$; (e) $\tilde{b} \to b\chi$.

Table 2
Topologies studied in the different scenarios

Production	Decay mode	Topology/Analysis	References
$\tilde{t}\bar{\tilde{t}}$	$\tilde{t} \to c\chi$ ($\Delta M \gtrsim 6$ GeV/c^2)	Acoplanar jets (AJ)	[1–3,5]
$\tilde{t}\bar{\tilde{t}}$	$\tilde{t} \to c/u\chi$ ($\Delta M \lesssim 6$ GeV/c^2)	Long-lived hadrons	[4]
$\tilde{t}\bar{\tilde{t}}$	$\tilde{t} \to b\chi f\bar{f}'$	Multi-jets (MJ)	This Letter
$\tilde{t}\bar{\tilde{t}}$	$\tilde{t} \to b\ell\tilde{\nu}$	AJ plus leptons	[1–3,5]
$\tilde{b}\bar{\tilde{b}}$	$\tilde{b} \to b\chi$	AJ plus b tagging	[1–3,5]
$\tilde{q}\bar{\tilde{q}}$	$\tilde{q} \to q\chi$	AJ	[2,3,5]

For stop masses accessible at LEP, i.e., $\lesssim 100$ GeV/c^2, the decay mode $\tilde{t} \to b\chi f\bar{f}'$ is mediated by virtual chargino and W (Fig. 1(b)) or sfermion (Fig. 1(c)) exchange. It is therefore of the same order in perturbation theory as the loop-induced $\tilde{t} \to c\chi$ decay, and can be substantially enhanced if charginos have masses not much larger than their present experimental bounds, and could even dominate for light sfermions [11]. The four-body decay channel yields topologies with b-jets, additional jets and/or leptons, and with missing mass and missing energy. A new multi-jet analysis, hereafter called MJ, has been designed to cope with these final states.

The $\tilde{t} \to b\ell\tilde{\nu}$ channel proceeds via virtual chargino exchange (Fig. 1(d)) and has a width of the order of 0.1–10 keV [10]. This decay channel dominates when it is kinematically allowed, i.e., if the lightest $\tilde{\nu}$ is lighter than the stop. If the lightest neutralino is the LSP, the sneutrino decays invisibly into $\chi\nu$ without any change in the experimental topology.

Under the assumption that the $\tilde{b}$ is lighter than all supersymmetric particles except the χ, the $\tilde{b}$ will decay as $\tilde{b} \to b\chi$ (Fig. 1(e)). Compared to the $\tilde{t}$, the $\tilde{b}$ decay width is larger, of the order of 10–100 MeV.

The supersymmetric partners of the light quarks are generally expected to be quite heavy. If they are light enough to be within the reach of LEP, their dominant decay mode is expected to be $\tilde{q} \to q\chi$.

The final state topologies addressed by the searches presented in this Letter are summarised in Table 2, together with the related signal processes and with the references where analysis details can be found.

This Letter is organised as follows. In Section 2, the ALEPH detector and the simulated samples used for the analyses are described. Section 3 is dedicated to the selection algorithms with emphasis on the new search for four-body stop decays. In Section 4 the results of the searches are given, along with their interpretation in the theoretical framework. The conclusions of the Letter are given in Section 5.

2. ALEPH detector and event simulation

A thorough description of the ALEPH detector and of its performance, as well as of the standard reconstruction and analysis algorithms, can be found in Refs. [12,13]. Only a brief summary is given here.

The trajectories of charged particles are measured by a silicon vertex detector (VDET), a cylindrical multi-wire drift chamber (ITC) and a large time projection chamber (TPC). These detectors are immersed in an axial magnetic field of 1.5 T provided by a superconducting solenoidal coil. The VDET consists of two cylindrical layers of silicon microstrip detectors; it performs precise measurements of the impact parameter in space, yielding powerful short-lived particle tags, as described in Ref. [14].

The electromagnetic calorimeter (ECAL), placed between the TPC and the coil, is a highly-segmented sandwich of lead planes and proportional wire chambers. It consists of a barrel and two endcaps. The hadron calorimeter (HCAL) consists of the iron return yoke of the magnet instrumented with streamer tubes. It is surrounded by two double layers of streamer tubes, the muon chambers. The luminosity monitors (LCAL and SiCAL) extend the calorimeter hermeticity down to 34 mrad from the beam axis.

The energy flow algorithm described in Ref. [13] combines the measurements of the tracking detectors and of the calorimeters into "objects" classified as charged particles, photons, and neutral hadrons. The energy resolution achieved with this algorithm is $(0.6\sqrt{E} + 0.6)$ GeV (E in GeV). Electrons are identi-

fied by comparing the energy deposit in ECAL to the momentum measured in the tracking system, by using the shower profile in the electromagnetic calorimeter, and by the measurement of the specific ionization energy loss in the TPC. The identification of muons makes use of the hit pattern in HCAL and of the muon chambers.

Signal event samples were simulated with the generator described in Ref. [1] for $\tilde{t} \to c\chi$, $\tilde{b} \to b\chi$, $\tilde{q} \to q\chi$ and $\tilde{t} \to b\ell\tilde{\nu}$. A modified version of this generator was designed to simulate the channel $\tilde{t} \to b\chi f\bar{f}'$, where the final state is modelled according to phase space and including parton shower development. The generation of $\tilde{t} \to c/u\chi$ with lifetime follows the procedure described in Ref. [4].

To simulate the relevant Standard Model background processes, several Monte Carlo generators were used: BHWIDE [15] for Bhabha scattering, KORALZ [16] for $\mu^+\mu^-$ and $\tau^+\tau^-$ production, PHOT02 [17] for $\gamma\gamma$ interactions, KORALW [18] for WW production, and PYTHIA [19] for the other processes ($e^+e^- \to q\bar{q}(\gamma)$, We$\nu$, Zee, ZZ, Z$\nu\bar{\nu}$). The sizes of the simulated samples typically correspond to ten times the integrated luminosity of the data.

All background and signal samples were processed through the full detector simulation.

3. Event selections

Several selection algorithms have been developed to search for the topologies given in Table 2. All these channels are characterised by missing energy. The event properties depend significantly on ΔM, the mass difference between the decaying squark and the χ (or the $\tilde{\nu}$ in the case of $\tilde{t} \to b\ell\tilde{\nu}$). When ΔM is large, there is a substantial amount of visible energy, and the signal events tend to look like WW, Weν, ZZ, and $q\bar{q}(\gamma)$ events. When ΔM is small, the visible energy is small, and the signal events are therefore similar to $\gamma\gamma$ events. In order to cope with the different signal topologies and background situations, each analysis employs selections dependent on the ΔM range. The stop lifetime may become sizeable at small ΔM, in which case the signal final state topology depends strongly on the $\tilde{t}$ decay length $\lambda_{\tilde{t}}$; three different selections are used, each designed to cope with a specific $\lambda_{\tilde{t}}$ range [4].

The optimisation of the selection criteria as well as the best combination of selections as a function of ΔM and $\lambda_{\tilde{t}}$ were obtained according to the $\overline{N}_{95}$ prescription [20], i.e., by minimisation of the 95% C.L. cross section upper limit expected in the absence of a signal. The selections are mostly independent of the centre-of-mass energy except for an appropriate rescaling of the cuts with $\sqrt{s}$ when relevant. The selections applied to the year 2000 data follow closely those described in Refs. [1–5] except for the new analysis developed to address the $\tilde{t} \to b\chi f\bar{f}'$ decay, hereafter described in some detail.

3.1. Search for $\tilde{t} \to b\chi f\bar{f}'$

The MJ analysis consists of a small, a large and a very large ΔM selection. These selections are designed to address simultaneously all $b\chi q\bar{q}'$ and $b\chi\ell\nu$ final states, independently of the decay branching ratios. The selections use several anti-$\gamma\gamma$ criteria, reported in Table 3. The cuts are derived from the AJ selection, described in Ref. [1] as well as the variables used. Only the relevant differences are discussed in the following.

In the $\tilde{t} \to b\chi f\bar{f}'$ channel, the b quark in the final state produces a visible mass higher than in the $\tilde{t} \to c\chi$ channel. Therefore, for the small ΔM selection, the cut on the number of charged particle tracks N_{ch} is reinforced by requiring $N_{\mathrm{ch}} > 10$, and both the visible mass, M_{vis}, and the visible mass computed excluding the leading lepton, $M_{\mathrm{vis}}^{\mathrm{ex}\,\ell_1}$, are required to be greater than 10 GeV/c^2. These tighter cuts allow others to be loosened: the transverse momentum p_{t} and that calculated excluding the neutral hadrons, $p_{\mathrm{t}}^{\mathrm{ex\,NH}}$, must be greater than $0.005\sqrt{s}$ and $0.01\sqrt{s}$, respectively. The remaining background is reduced in the small ΔM selection by requiring the thrust to be smaller than 0.875, and by the cut $E_{\mathrm{vis}} < 0.26\sqrt{s}$.

For the large ΔM selections, the multi-jet signature is addressed by requiring y_{45}, as calculated with the DURHAM algorithm [21], to be greater than 0.001. The level of the WW, ZZ and Weν background is reduced by taking advantage of the b-quark content in the $\tilde{t} \to b\chi f\bar{f}'$ final state. The value of $-\log_{10} P_{\mathrm{uds}}$ is required to be greater than 0.5, where P_{uds} is the b-tag event probability introduced in Ref. [14]. This background is further suppressed

Table 3
Criteria used in the MJ selections to address the backgrounds from (A) $\gamma\gamma \to q\bar{q}$, (B) $\gamma\gamma \to q\bar{q}$ with spurious calorimetric objects and (C) $\gamma\gamma \to \tau^+\tau^-$. The † indicates that the cut is applied when the azimuthal angle of the missing momentum $\phi_{\vec{p}_{\rm miss}}$ is within 15° of the vertical plane

		Small ΔM		Large and very large ΔM
A	$N_{\rm ch}$		> 10	
	$M_{\rm vis}$		> 10 GeV/c^2	
	E_{12°	$= 0$		$< 0.05\sqrt{s}$
	E_{30°	$< 0.25E_{\rm vis}$		$< 0.3E_{\rm vis}$
	$\Phi_{\rm acop}$ (acoplanarity)	$< 172.5^\circ$		$< 174^\circ$
	$\Phi_{\rm acop_T}$ (transverse acop.)	$< 175^\circ$		$< 75^\circ$
	$p_{\rm t}/\sqrt{s}$	> 0.005 (> 0.01)†		> 0.05 (> 0.075)†
	$p_{\rm t}/E_{\rm vis}$	$> 1.305 - 0.00725\Phi_{\rm acop}$		> 0.2
	$M_{\rm miss}$	$< 25.0E_{\rm vis}$		
	$\theta_{\rm point}$	$> 15^\circ$		$> 5^\circ$ if $\theta_{\rm scat} < 15^\circ$
	$\lvert\cos\theta_{\vec{p}_{\rm miss}}\rvert$	< 0.8		< 0.95
	$\lvert\cos\theta_{\rm thrust}\rvert$	< 0.75		
	$M_{\rm vis}^{{\rm ex}\,\ell_1}$	> 10 GeV/c^2		
B	$p_{\rm t}^{\rm ex\,NH}$	$> 0.01\sqrt{s}$		$< 0.03\sqrt{s}$ if $E_{\rm vis}^{\rm NH} > 0.45E_{\rm vis}$
	$p_{\rm t}^{\rm ch}$	$> 0.005\sqrt{s}$		
	$E_1^{\rm NH}$	$< 0.3\sqrt{s}$		
	$E_{\rm vis}^{\rm NH}$			$< 0.3E_{\rm vis}$
	$E(\phi_{\vec{p}_{\rm miss}} \pm 15^\circ)$			$< 0.075\sqrt{s}$
C	$N_{\rm ch}^{{\rm jet}_i}$, $i = 1, 2$	> 4		
	$m^{{\rm jet}_i}$, $i = 1, 2$	> 4 GeV/c^2		

by a missing mass cut, the location of which is a function of the ΔM of the signal considered. For example, for $\Delta M = 20$, 30 and 40 GeV/c^2 the optimal cuts are $M_{\rm miss}/\sqrt{s} > 0.75$, 0.70 and 0.65, respectively.

The region where the very large ΔM selection applies is characterised by a higher visible mass. The sliding cut on the missing mass is looser than that in the large ΔM selection. For $\Delta M = 20$, 40 and 60 GeV/c^2 the optimal cuts are $M_{\rm miss}/\sqrt{s} > 0.58$, 0.34 and 0.10. Other cuts are then necessary to reduce the background mainly due to WW events. Similarly to the large ΔM case, $-\log_{10} P_{\rm uds}$ and y_{45} are required to be greater than 0.5 and 0.003, respectively. The mean momentum of all reconstructed charged particle tracks must be less than $0.007\sqrt{s}$. To reduce background from semileptonic W decays, the fraction of visible energy due to charged objects excluding the leading lepton is required to be greater than 0.5, and the leading lepton, if present, must not be isolated, i.e., the additional energy deposited in a 30° cone around its direction must be at least 50% of its energy. At this level, the remaining background consists of WW events with energy lost in the beam pipe, responsible for the missing mass. These events are rejected by requiring $|p_z| < 0.1\sqrt{s}$ and the energy E_{12° deposited at polar angle smaller than 12° to be less than $0.015\sqrt{s}$.

The efficiencies of the three selections were parametrised as a function of ΔM for each stop pair final state that may result from the decay channels considered ($\tilde{\rm t} \to {\rm c}\chi$, $\tilde{\rm t} \to {\rm b}\chi\ell\nu$, $\tilde{\rm t} \to {\rm b}\chi{\rm q}\bar{\rm q}'$). This allows the signal efficiency to be parametrised as a function of the branching ratios. The efficiencies were checked to be practically independent of the lepton flavour (e, μ, τ) in the $\tilde{\rm t} \to {\rm b}\chi\ell\nu$ decay. The small, large and very large ΔM selections are combined using the $\overline{\rm N}_{95}$ procedure as a function of ΔM and of the branching ratios. The background to the small ΔM selection is dominated by $\gamma\gamma \to q\bar{q}$ events and has a total expectation of 5.0 fb, while the backgrounds of the large and very large ΔM selections, dominated by WW and other four-fermion processes amount to 3.5 and 4.4 fb, respectively.

3.2. Systematic uncertainties

The efficiencies of the MJ analysis may be affected by uncertainties regarding the assumptions on the stop hadron physics and by uncertainties related to the detector response. The results of the systematic studies are summarised in Table 4 for the three selections.

The systematic effects from the assumptions on the stop hadron physics were assessed by varying the parameters of the model implemented in the generator as in Ref. [1]. The uncertainties from the stop hadron mass were evaluated by varying the effective spectator mass M_{eff}, set to 0.5 GeV/c^2 in the analysis, in the range between 0.3 and 1.0 GeV/c^2. The efficiencies of the large and very large ΔM selections are almost insensitive to this change. The 9% effect found for the small ΔM selection reflects the variation in the invariant mass available for the hadronic system.

The systematic error due to the uncertainty on the stop fragmentation was evaluated by varying $\epsilon_{\tilde{\mathrm{t}}}$ by an order of magnitude, where $\epsilon_{\tilde{\mathrm{t}}}$ is the parameter of the Peterson fragmentation function [22]. The effect on the efficiency is very small ($\sim 2\%$).

The amount of initial state radiation in stop pair production depends on the value of the stop coupling to the Z boson, which is controlled by the stop mixing angle. A variation of $\theta_{\tilde{\mathrm{t}}}$ from 56° to 0°, i.e., from minimal to maximal coupling, was applied. The effect was found to be small in all selections, at the level of 1 to 3%.

Detector effects have been studied for the variables used in the selections. The distributions of all relevant variables show good agreement with the simulation. In particular, the b-tagging performance was checked on hadronic events collected at the Z resonance. The systematic errors associated to detector effects and to the reconstruction procedure were found to be negligible.

Beam-related background, not included in the event simulation, may affect the E_{12° variable. Its effect on the selection efficiency was determined from data collected at random beam crossings. The net effect is a relative decrease of the signal efficiency by about 5%. The uncertainty on this correction is negligible.

Finally, an additional uncertainty of 3% due to the limited Monte Carlo statistics was added. The total systematic uncertainty is at the level of 10% for the small ΔM selection. It is dominated by the limited knowledge of the stop hadron physics, and results from rather extreme changes in the model parameters. The systematic uncertainties for the large and very large ΔM selections are at the level of 4–5%.

The systematic uncertainties in the selections other than for the $\tilde{\mathrm{t}} \to \mathrm{b}\chi\mathrm{f}\bar{\mathrm{f}}'$ channel are essentially identical to those reported in Refs. [4,5].

4. Results and interpretation

The numbers of candidate events selected and background events expected are reported in Table 5 for all the data samples used to derive the results below. An overall agreement is observed. In particular, a total of six candidate events is selected by the new MJ analysis, with 8.5 events expected from background processes; two events are found by each of the selections, in agreement with predictions of 3.3, 2.3 and 2.9 background events at small, large and very large ΔM, respectively.

In the framework of the supersymmetric extension of the Standard Model [9], the outcome of these searches can be translated into constraints in the

Table 4
Summary of the relative systematic uncertainties (%) on the efficiencies of the MJ analysis

	MJ selections		
	Small ΔM	Large ΔM	Very large ΔM
M_{eff} (0.3–1.0 GeV)	9	2	3
$\epsilon_{\tilde{\mathrm{t}}}$ (10^{-5}–10^{-4})	2	2	2
$\theta_{\tilde{\mathrm{t}}}$ (0°–56°)	3	1	1
Detector and reconstruction	2	1	2
Monte Carlo statistics	3	3	3
Total	10	4	5

Table 5
Numbers of candidate events observed (N_{obs}) and expected from background (N_{exp}) for the different selections. Also given are the sizes ($\int \mathcal{L}\,dt$) and the average centre-of-mass energies $\langle\sqrt{s}\rangle$ of the samples analysed

Sample	Year	1997		1998		1999		2000	
	$\int \mathcal{L}\,dt$ (pb^{-1})	57.0		173.6		236.9		207.3	
	$\langle\sqrt{s}\rangle$ (GeV)	182.7		188.6		197.6		206.2	
Analysis	Selection	N_{obs}	N_{exp}	N_{obs}	N_{exp}	N_{obs}	N_{exp}	N_{obs}	N_{exp}
AJ	Small ΔM	1	1.5	3	5.5	2	2.4	2	2.1
	Large ΔM	4	3.5	5	4.0	8	7.3	11	8.6
Long-lived hadrons	Small $\lambda_{\tilde{t}}$				AJ, small ΔM				
	Intermediate $\lambda_{\tilde{t}}$	–	–	0	0.3	0	0.5	0	0.4
	Large $\lambda_{\tilde{t}}$	–	–	1	0.4	0	0.6	0	0.6
MJ	Small ΔM	0	0.3	1	0.7	1	1.2	0	1.1
	Large ΔM	1	0.2	0	0.6	0	0.8	1	0.7
	Very large ΔM	0	0.2	0	0.8	1	1.0	1	0.9
AJ Plus leptons	Small ΔM	1	0.8	0	1.9	3	2.6	0	2.4
	Large ΔM	0	0.1	2	0.4	2	1.4	3	1.6
AJ plus b-tagging	Small ΔM	0	1.1	3	3.3	1	2.2	2	2.0
	Large ΔM	1	0.6	0	0.9	1	0.7	0	1.2

space of the relevant parameters. In this process the systematic uncertainties on the selection efficiencies were included according to the method described in Ref. [23], and no background subtraction was applied. The constraints discussed below, derived from the results given in Table 5, are at 95% confidence level.

The regions excluded in the plane $(M_{\tilde{t}}, M_{\chi})$ under the hypothesis of a dominant $\tilde{t} \to c/u\chi$ decay are shown in Fig. 2(a) for two values of the $\tilde{t}$ mixing angle $\theta_{\tilde{t}}$, 0° and 56°, corresponding to maximal and vanishing $\tilde{t}\tilde{t}Z$ coupling, respectively. For 8 GeV/c^2 < $\Delta M < M_W + M_b$, and using also CDF results [24], the lower limit on $M_{\tilde{t}}$ is 92 GeV/c^2, independent of $\theta_{\tilde{t}}$.

The very small ΔM corridor is partially covered by the "long-lived hadrons" analysis as indicated by the plain dark region in Fig. 2(a). The stop mass lower limit provided by the "long-lived hadrons" analysis is shown in Fig. 2(b) as a function of $\log(c\tau_{\tilde{t}}/\text{cm})$ for various ΔM values. The smallest ΔM value considered is 1.6 GeV/c^2, corresponding to the "effective" kinematic limit for the decay $\tilde{t} \to c\chi$ [4]. Below that ΔM value, the stop decay mode is $\tilde{t} \to u\chi$, and the limit is 95 GeV/c^2, given by the large lifetime selection. The absolute mass lower limit obtained is 63 GeV/c^2. It is reached for $\Delta M = 1.6$ GeV/c^2 and for a $c\tau_{\tilde{t}}$ value of ~ 1 cm. In that configuration of parameters, the "AJ small ΔM" and the "long-lived hadrons intermediate lifetime" selections are combined.

In the MSSM [9], more restrictive constraints on the stop mass can be obtained since ΔM and the stop lifetime are related. The mass lower limit obtained by scanning over the relevant model parameters as in Ref. [4] is shown in Fig. 2(c) as a function of $\tan\beta$. For any $\tan\beta$, the stop mass limit is 65 GeV/c^2, reached for $\tan\beta \sim 2.7$.

Under the hypothesis that the decay $\tilde{t} \to b\chi f\bar{f}'$ is dominant, the regions excluded in the plane $(M_{\tilde{t}}, M_{\chi})$ are shown in Fig. 3(a), for relative proportions of the possible $f\bar{f}'$ final states as in W* decays. In Fig. 3(b) the leptonic modes $b\chi\ell\nu$ (with equal branching ratios for $\ell = e$, μ and τ) are assumed to be dominant. The excluded regions are given for $\theta_{\tilde{t}} = 0°$ and $\theta_{\tilde{t}} = 56°$. For $\Delta M > 8$ GeV/c^2, the $\theta_{\tilde{t}}$-independent lower limits on $M_{\tilde{t}}$ are 78 GeV/c^2 and 80 GeV/c^2, for the two cases of W* and leptonic final state dominance, respectively.

The combination of the AJ and MJ analyses allows constraints to be set under the more general hypothesis that both the $\tilde{t} \to c\chi$ and $\tilde{t} \to b\chi f\bar{f}'$ decay channels contribute to stop decays. The excluded regions in the plane $(M_{\tilde{t}}, M_{\chi})$ are shown in Fig. 4(a) for $\theta_{\tilde{t}} = 0°$and $\theta_{\tilde{t}} = 56°$. This result was obtained by arbitrarily varying the $\tilde{t} \to c\chi$ branching ratio and the leptonic frac-

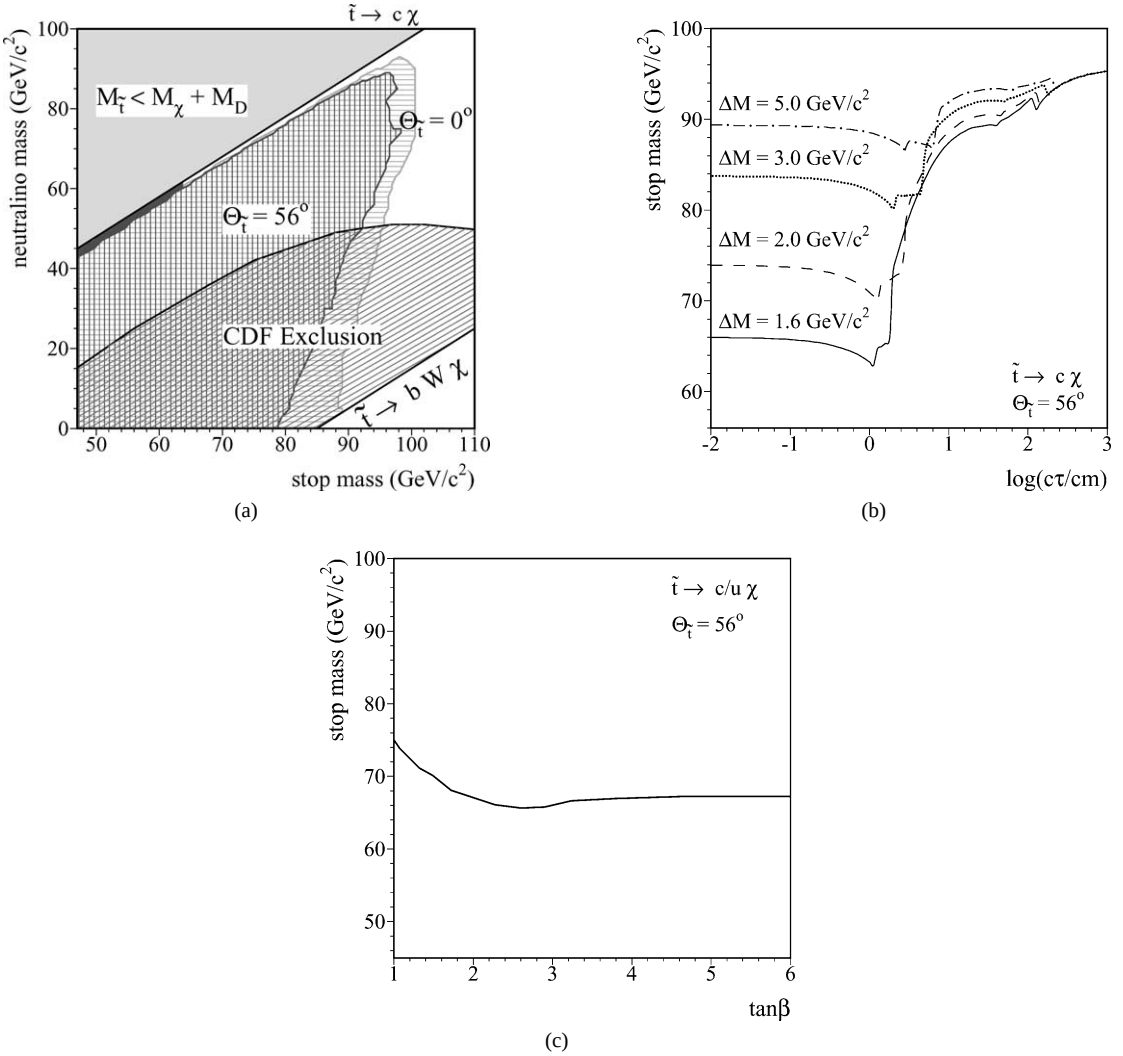

Fig. 2. (a) Excluded regions at 95% C.L. in the M_χ vs. $M_{\tilde{t}}$ plane from $\tilde{t} \to c/u\chi$ searches; the excluded regions are given for $\theta_{\tilde{t}} = 0°$, corresponding to maximum $\tilde{t}\tilde{t}Z$ coupling, and for $\theta_{\tilde{t}} = 56°$, corresponding to vanishing $\tilde{t}\tilde{t}Z$ coupling. The dark region in the small ΔM corridor is excluded by the "long-lived hadrons" analysis. The CDF experiment result is also indicated. (b) Stop mass lower limit at 95% C.L. from the "long-lived hadrons" as a function of $\log(c\tau_{\tilde{t}}/\mathrm{cm})$ for several ΔM values, without any assumption on the relation between ΔM and the stop lifetime $\tau_{\tilde{t}}$. (c) Stop mass lower limit at 95% C.L. from the "long-lived hadrons" analysis as a function of $\tan\beta$, independent of the other MSSM parameters.

tion in the $\tilde{t} \to b\chi f\bar{f}'$ decay, and by using the $\overline{N}_{95}$ prescription to determine the appropriate combination of selections. The stop mass limit is shown in Fig. 4(b) as a function of the branching ratio $\mathrm{BR}(\tilde{t} \to c\chi)$ for several fixed ΔM values and for $\theta_{\tilde{t}} = 56°$. The smallest ΔM value considered is 5 GeV/c^2, corresponding to the threshold for the production of a b quark in the final state. The lowest limit obtained is 63 GeV/c^2; it is reached for $\Delta M = 5$ GeV/c^2, $\mathrm{BR}(\tilde{t} \to c\chi) = 0.22$, and $\mathrm{BR}(\tilde{t} \to b\chi\ell\nu) = 0.55$.

Under the assumption that the $\tilde{t} \to b\ell\tilde{\nu}$ decay mode is dominant, with equal branching ratios for $\ell = e$, μ and τ, the excluded region in the plane $(M_{\tilde{t}}, M_{\tilde{\nu}})$ is shown in Fig. 5(a). If $\Delta M > 8$ GeV/c^2, and using the LEP1 limit on the sneutrino mass and D0 results [25], the lower limit on $M_{\tilde{t}}$ is 97 GeV/c^2, independent of $\theta_{\tilde{t}}$.

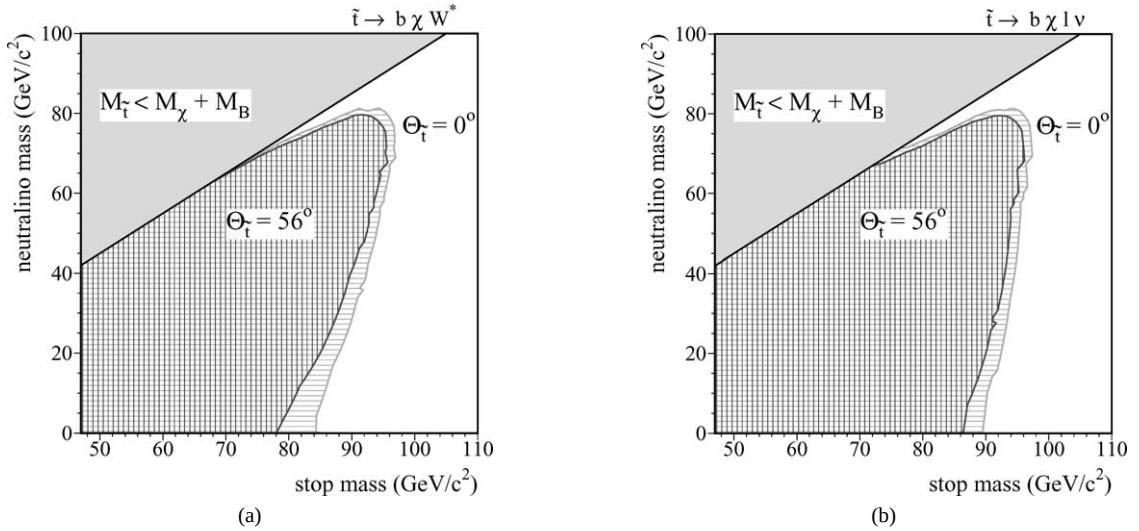

Fig. 3. Excluded regions at 95% C.L. in the M_χ vs. $M_{\tilde{t}}$ plane from $\tilde{t} \to b\chi f\bar{f}'$ searches: (a) the W* modes or (b) the leptonic modes are assumed to be dominant for the $f\bar{f}'$ final states. The excluded regions are given for $\theta_{\tilde{t}} = 0°$, corresponding to maximum $\tilde{t}\tilde{t}Z$ coupling, and for $\theta_{\tilde{t}} = 56°$, corresponding to vanishing $\tilde{t}\tilde{t}Z$ coupling.

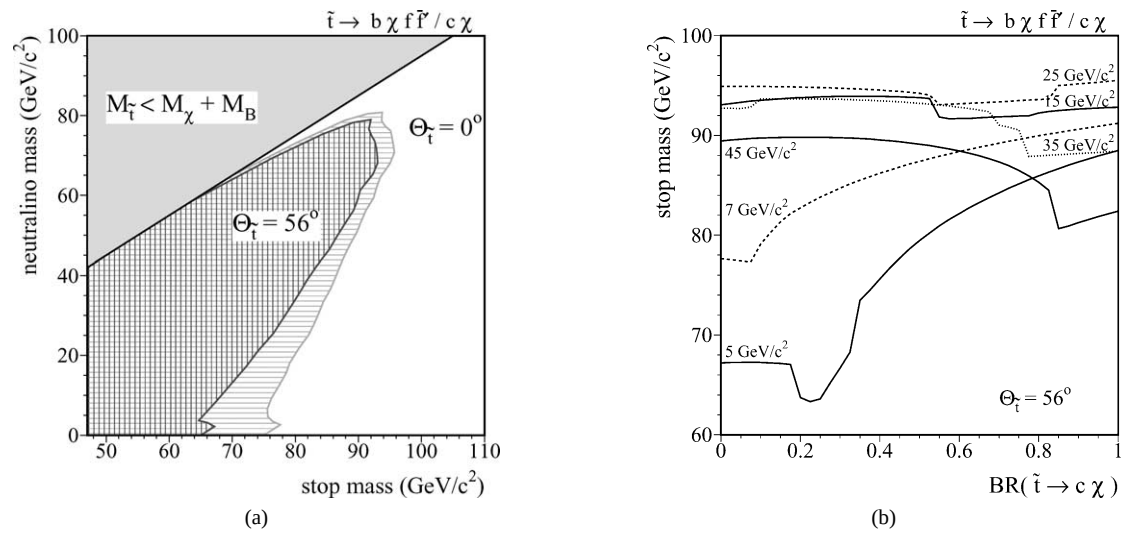

Fig. 4. (a) Branching ratio independent excluded regions at 95% C.L. in the M_χ vs. $M_{\tilde{t}}$ plane, from $\tilde{t} \to b\chi f\bar{f}'$ and $\tilde{t} \to c\chi$ searches. The excluded regions are given for $\theta_{\tilde{t}} = 0°$, corresponding to maximum $\tilde{t}\tilde{t}Z$ coupling, and for $\theta_{\tilde{t}} = 56°$, corresponding to vanishing $\tilde{t}\tilde{t}Z$ coupling. (b) Limit on the stop mass at 95% C.L. as a function of BR($\tilde{t} \to c\chi$) for various ΔM values. The limits are given for $\theta_{\tilde{t}} = 56°$.

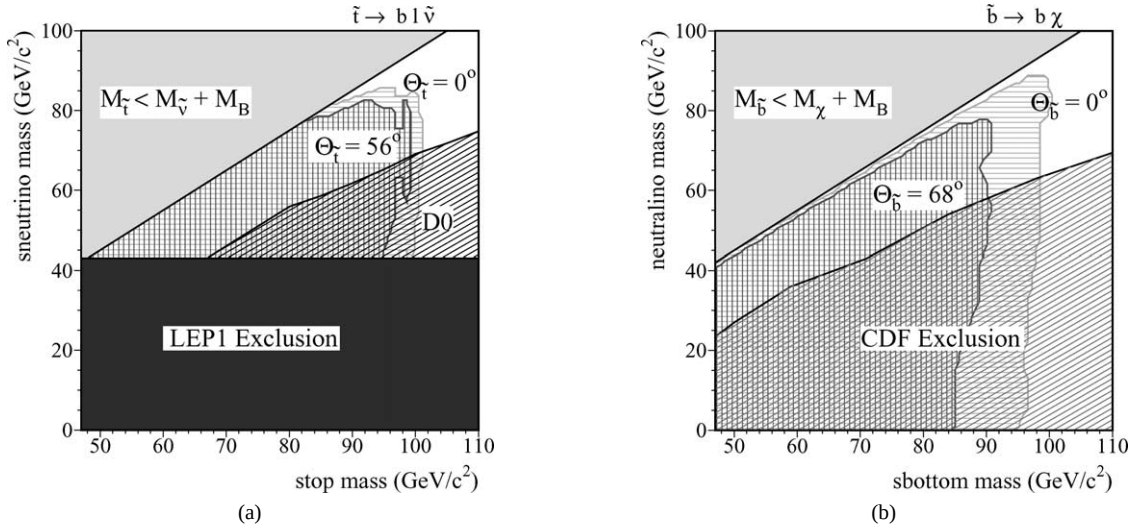

Fig. 5. (a) Excluded regions at 95% C.L. in the $M_{\tilde{\nu}}$ vs. $M_{\tilde{t}}$ plane from $\tilde{t} \to b\ell\tilde{\nu}$ searches (equal branching fractions for the $\tilde{t}$ decay to e, μ, and τ are assumed). The excluded regions are given for $\theta_{\tilde{t}} = 0°$, corresponding to maximum $\tilde{t}\tilde{t}Z$ coupling, and for $\theta_{\tilde{t}} = 56°$, corresponding to vanishing $\tilde{t}\tilde{t}Z$ coupling. The regions excluded at LEP 1 and by the D0 experiment are also indicated. (b) Excluded regions at 95% C.L. in the M_{χ} vs. $M_{\tilde{b}}$ plane from $\tilde{b} \to b\chi$ searches. The excluded regions are given for $\theta_{\tilde{b}} = 0°$, corresponding to maximum $\tilde{b}\tilde{b}Z$ coupling, and for $\theta_{\tilde{b}} = 68°$, corresponding to vanishing $\tilde{b}\tilde{b}Z$ coupling. The region excluded by the CDF experiment is also indicated.

The lower limit is 82 GeV/c^2 if the $\tilde{t} \to b\tau\tilde{\nu}_\tau$ decay mode is dominant and $\Delta M > 8$ GeV/c^2, independent of $\theta_{\tilde{t}}$.

The excluded region in the plane $(M_{\tilde{b}}, M_{\chi})$ is shown in Fig. 5(b) under the assumption of a dominant $\tilde{b} \to b\chi$ decay. Taking also the CDF exclusion [24] into account, a lower limit of 89 GeV/c^2 is set on $M_{\tilde{b}}$, for any $\tilde{b}$ mixing angle and $\Delta M > 8$ GeV/c^2. The region excluded for $\theta_{\tilde{b}} = 0°$, for which the $\tilde{b}\tilde{b}Z$ coupling is maximal, is also shown.

As discussed in detail in Ref. [2], the results of the search for acoplanar jets, with or without b-tagging, can also be translated into constraints on the mass of degenerate squarks. In order to compare these results with those obtained at the Tevatron [24,25], limits have been evaluated within the MSSM [9] under the following assumptions: a degenerate mass $M_{\tilde{q}}$ for all left-handed and right-handed $\tilde{u}$, $\tilde{d}$, $\tilde{c}$, $\tilde{s}$, $\tilde{b}$ squarks; lowest order GUT relation between the soft supersymmetry breaking gaugino mass terms, allowing the gluino and neutralino masses to be related; $\tan\beta = 4$ and $\mu = -400$ GeV. The results in the plane $(M_{\tilde{g}}, M_{\tilde{q}})$ are shown in Fig. 6. Improved constraints are obtained in the region of small $\tilde{q}$ to χ mass differences.

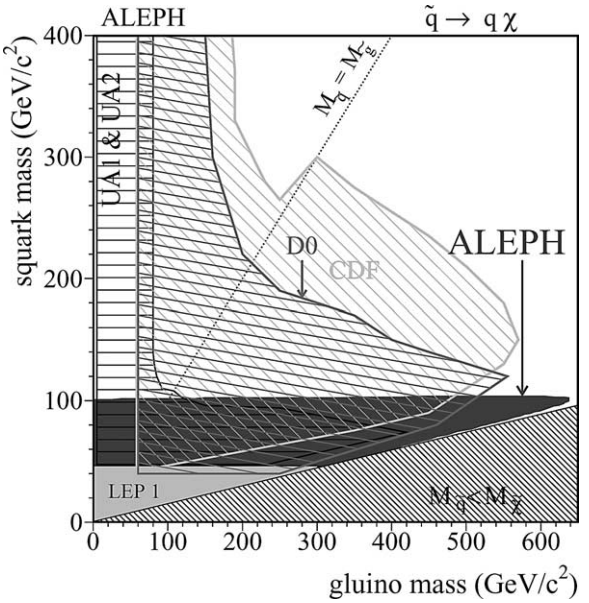

Fig. 6. Excluded regions at 95% C.L. from the search for generic $\tilde{q}$ pairs, assuming five mass-degenerate $\tilde{q}$ flavours. The results are shown in the gluino–squark mass plane for $\tan\beta = 4$ and $\mu = -400$ GeV, together with results from experiments at $p\bar{p}$ colliders.

Table 6
Lower limits on stop and sbottom masses in some relevant cases. All limits are valid for any value of the mixing angle

Squark	95% C.L. Mass limit (GeV/c^2)	ΔM range (GeV/c^2)	Dominant decay channel(s)	Comments
$\tilde{\mathrm{t}}$	92	> 8	$\tilde{\mathrm{t}} \to \mathrm{c}\chi$	CDF result [24] used
	78	> 8	$\tilde{\mathrm{t}} \to \mathrm{b}\chi\mathrm{W}^*$	
	97	> 8	$\tilde{\mathrm{t}} \to \mathrm{b}\ell\tilde{\nu}$	LEP 1, D0 result [25] used
	63	Any	Any	Any branching ratios, any lifetime
$\tilde{\mathrm{b}}$	89	> 8	$\tilde{\mathrm{b}} \to \mathrm{b}\chi$	CDF result [24] used

5. Conclusions

Searches for signals of pair-produced scalar partners of quarks have been performed in the data sample of 207 pb^{-1} collected in the year 2000 with the ALEPH detector at LEP, at centre-of-mass energies ranging from 204 to 209 GeV. The final state topologies studied arise from the decays $\tilde{\mathrm{t}} \to \mathrm{c}/\mathrm{u}\chi$, $\tilde{\mathrm{t}} \to \mathrm{b}\chi\mathrm{f}\bar{\mathrm{f}}'$, $\tilde{\mathrm{t}} \to \mathrm{b}\ell\tilde{\nu}$, $\tilde{\mathrm{b}} \to \mathrm{b}\chi$, and $\tilde{\mathrm{q}} \to \mathrm{q}\chi$. The four-body stop decay channel was analysed for the first time at LEP, and the corresponding selections were extended to the 675 pb^{-1} of data collected by ALEPH at centre-of-mass energies of 183 GeV and above. All numbers of candidate events observed are consistent with the backgrounds expected from Standard Model processes. The results of these searches, combined with earlier ones obtained with data collected from 1997 to 1999, have been translated into improved mass lower limits, of which relevant examples are given in Table 6. In particular, a 95% C.L. lower limit of 63 GeV/c^2 has been set on the stop mass, irrespective of its lifetime and decay branching ratios.

Acknowledgements

We wish to congratulate our colleagues from the accelerator divisions for the successful operation of LEP at high energies. We would also like to express our gratitude to the engineers and support people at our home institutes without whom this work would not have been possible. Those of us from non-member states wish to thank CERN for its hospitality and support.

References

[1] ALEPH Collaboration, Phys. Lett. B 413 (1997) 431.
[2] ALEPH Collaboration, Phys. Lett. B 434 (1998) 189.
[3] ALEPH Collaboration, Phys. Lett. B 469 (1999) 303.
[4] ALEPH Collaboration, Phys. Lett. B 488 (2000) 234.
[5] ALEPH Collaboration, Phys. Lett. B 499 (2001) 67.
[6] DELPHI Collaboration, Phys. Lett. B 489 (2000) 38.
[7] L3 Collaboration, Phys. Lett. B 471 (1999) 308.
[8] OPAL Collaboration, Phys. Lett. B 456 (1999) 95.
[9] H.P. Nilles, Phys. Rep. 110 (1984) 1;
H.E. Haber, G.L. Kane, Phys. Rep. 117 (1985) 75;
R. Barbieri, Riv. Nuovo Cimento 11N4 (1988) 1.
[10] K. Hikasa, M. Kobayashi, Phys. Rev. D 36 (1987) 724;
M. Drees, K. Hikasa, Phys. Lett. B 252 (1990) 127.
[11] C. Boehm, A. Djouadi, Y. Mambrini, Phys. Rev. D 61 (2000) 095006.
[12] ALEPH Collaboration, Nucl. Instrum. Methods A 294 (1990) 121.
[13] ALEPH Collaboration, Nucl. Instrum. Methods A 360 (1995) 481.
[14] ALEPH Collaboration, Phys. Lett. B 313 (1993) 535.
[15] S. Jadach, W. Placzek, B.F. Ward, Phys. Lett. B 390 (1997) 298.
[16] S. Jadach, B.F. Ward, Z. Wąs, Comput. Phys. Commun. 79 (1994) 503.
[17] J.A.M. Vermaseren, Two gamma physics versus one gamma physics and whatever lies in between, in: G. Cochard, P. Kessler (Eds.), Proceedings of the IVth international Workshop on Gamma–Gamma Interactions, Springer, Berlin, 1980;
ALEPH Collaboration, Phys. Lett. B 313 (1993) 509.
[18] S. Jadach, W. Placzek, M. Skrzypek, B.F. Ward, Z. Wąs, Comput. Phys. Commun. 119 (1999) 272.
[19] T. Sjöstrand, Comput. Phys. Commun. 82 (1994) 74.
[20] ALEPH Collaboration, Phys. Lett. B 313 (1993) 299;
J.F. Grivaz, F. Le Diberder, Complementary analyses and acceptance optimization in new particle searches, LAL 92-37 (1992).
[21] W.J. Stirling, J. Phys. G 17 (1991) 1567.
[22] C. Peterson, D. Schlatter, I. Schmitt, P.M. Zerwas, Phys. Rev. D 27 (1983) 105.
[23] R.D. Cousins, V.L. Highland, Nucl. Instrum. Methods A 320 (1992) 331.
[24] CDF Collaboration, Phys. Rev. Lett. 84 (2000) 5704;

CDF Collaboration, Phys. Rev. Lett. 84 (2000) 5273;
CDF Collaboration, Phys. Rev. Lett. 88 (2002) 041801.
[25] D0 Collaboration, Phys. Rev. Lett. 75 (1995) 618;
D0 Collaboration, Phys. Rev. Lett. 83 (1999) 4937;
D0 Collaboration, Phys. Rev. D Rapid Comm. 60 (1999) 031101;
D0 Collaboration, hep-ex/0108018, submitted to Phys. Rev. Lett., 2001.